Research Square

Preprints are preliminary reports that have not undergone peer review.
They should not be considered conclusive, used to inform clinical practice,
or referenced by the media as validated information.

Dynamic-Static Coordination-Crosslinked Hybrid Polyimides with Ultrahigh Thermal Stability and Closed-Loop Recyclability

Rui Shang
Donghua University
Peiyan Zhang
Donghua University
Di Wu
Shazhou Professional Institute of Technology
Xiuting Li
lixiuting@dhu.edu.cn

Donghua University
Xin Zhao
Donghua University
Jie Dong
Donghua University
Qinghua Zhang
Donghua University

Research Article

Keywords:

Posted Date: August 6th, 2026

DOI: https://doi.org/10.21203/rs.3.rs-9877415/v1

License: This work is licensed under a Creative Commons Attribution 4.0 International License.
Read Full License

Additional Declarations: No competing interests reported.

Dynamic-Static Coordination-Crosslinked Hybrid Polyimides with Ultrahigh Thermal Stability and Closed-Loop Recyclability

Rui Shang[1,2]· Peiyan Zhang[1]· Di Wu[3]· Xiuting Li[1,2]· Xin Zhao[1*]· Jie Dong[1]· Qinghua Zhang[1]*

[1] State Key Laboratory of Advanced Fiber Materials, College of Materials Science and Engineering, Donghua University, Shanghai, 201620, China

[2] Shanghai Key Laboratory of Lightweight Composite, Donghua University，Shanghai 201620, China

[3] Textile and Clothing Materials College, Shazhou Professional Institute of Technology, Suzhou, 215600, China

**Email: lixiuting@dhu.edu.cn; xzhao@dhu.edu.cn*

Abstract

Cross-linking endows polymers with the thermal stability, rigidity, and solvent resistance required for extreme environments, yet the permanently locked networks that enable these properties inherently prohibit reprocessing and closed-loop recyclability. Herein, we report a dynamic-static coordination hybrid polyimide constructed through Cu^{2+}–benzimidazole interactions within a rigid aromatic backbone, where bulky $–CF_3$ groups adjacent to the coordination sites create localized free volume that promotes segmental motion and enables thermally triggered bond exchange. The optimized PI–Cu50% network achieves a record-high glass transition temperature of 430 °C among dynamic polymer networks, together with a Young's modulus of 4.4 GPa, tensile strength of 128 MPa, and excellent fatigue resistance with residual strain below 0.5% after 20 cycles. Upon heating to ~200 °C, the coordination network transitions from a quasi-static state into a dynamically adaptive state, where the elongation at break increases nearly tenfold while maintaining superior strength and stiffness. The constrained coordination environment further suppresses ion migration and dipolar relaxation, enabling low dielectric loss, a high breakdown strength of 514 MV/m, and stable dielectric performance from −150 to 250 °C. Despite its highly cross-linked character and excellent solvent resistance, the coordination network can be selectively dissociated by a competitive ligand, enabling complete recycling with over 99% tensile-strength retention after regeneration. This work establishes a dynamic-static coordination hybrid strategy that reconciles thermoset-level performance with closed-loop recyclability under extreme conditions.

1 Introduction

Polymer dielectric films play a crucial role in advanced technological fields such as flexible electronics, high-power electrical systems, and aerospace insulation, where exceptional thermal stability, mechanical strength, and dielectric reliability are required[1, 2]. Polyimides (PIs) are highly favored in these applications due to their inherent high temperature resistance and excellent mechanical properties[3, 4]. However, conventional polyimides are difficult to reprocess or recycle once cured. To improve their processability, researchers have developed thermoplastic polyimides by introducing flexible segments or bulky side groups[5]. Although such materials can be repeatedly melt- or solvent-processed, their high-temperature resistance is generally compromised by the flexible ether, ketone linkages or bulky side groups required to impart melt processability, limiting service temperatures to below 300 °C[6]. Consequently, developing polyimide materials that combine excellent heat resistance with good recyclability has remained a significant research focus in this field[7].

Dynamic covalent chemistry has redefined the thermoset/thermoplastic dichotomy through vitrimers: permanently cross-linked networks that undergo stress relaxation and reprocessing without compromising structural integrity. Since Leibler's seminal demonstration of associative exchange in epoxy systems in 2011[8], this mechanism has been systematically extended to polyesters, polyurethanes and polyolefins, establishing a universal platform for recyclable high-performance polymers. However, their high-temperature application remains fundamentally limited: dynamic bond exchange requires sufficient chain mobility, which is typically achieved at temperatures approaching or exceeding the glass-transition temperature (T_g). Meanwhile, common dynamic bonds (e.g., hydrogen bonds[9, 10], disulfide bonds[11, 12], imine bonds[13-16], and Diels-Alder bonds[17, 18]) often exhibit inadequate thermal stability at elevated temperatures, tending to undergo premature dissociation or irreversible cleavage. As a result, the long-term service temperature of most vitrimers is generally confined to below 300 °C, a limitation inherently governed by the trade-off between exchange activity and the structural stability of the dynamic bonds.

Metal-coordination bonds represent a class of dynamic interactions formed between organic ligands and metal ions. Their bond dissociation energies typically range from 80 to 350 kJ/mol, situating their strength strategically between that of hydrogen bonds (0-20 kJ/mol) and covalent bonds[19]. The exact bond strength can be finely tuned through precise selection of metal ions and

modulation of ligand structures[20, 21]. Moreover, these bonds are capable of reversibly re-forming after rupture, thereby endowing materials with dynamic, tunable, and even self-healing mechanical properties[22, 23]. This combination of characteristics makes metal-coordination bonds an ideal platform for constructing polymer networks that integrate high thermal stability with dynamic responsiveness. For instance, incorporating α-diimide ligands into a polyimide backbone followed by coordination with Cu^{2+} has been shown to improve the thermal resistance and dimensional stability of the resulting films[24]. However, the T_g of such systems generally remain below 400 °C, highlighting an inherent limitation of conventional coordination designs in reconciling high-temperature stability with dynamic reversibility, which restricts their application in extreme thermal environments such as aerospace and deep-earth exploration.

To ensure thermal stability, a high-density metal-coordination network was constructed within the rigid polymer backbones. Concurrently, bulky flexible side groups were introduced in the vicinity of the coordination sites. These side groups created sufficient free volume for chain movement, which facilitated the dynamic dissociation and reorganization of the coordination bonds under heating. As a result, the material achieved both exceptional heat resistance and desirable reprocessability. Specifically, benzimidazole ligand units were embedded directly into the rigid aromatic backbone of a polyimide, enabling the construction of a thermally stable, chain-interconnected coordination network with Cu^{2+} ions. Concurrently, bulky trifluoromethyl (CF_3) groups were introduced near the coordination centers to maintain network dynamics. Moreover, using ethylenediaminetetraacetic acid (EDTA) as a strong competitive ligand enabled the efficient and controllable disassembly of the coordination-crosslinked polyimide into its linear form, achieving closed-loop recovery. This work not only validates the feasibility of synergistically enhancing thermal stability and dynamic reversibility at the molecular level but also provides a novel design paradigm and a practical material platform for developing high-performance, sustainable polymers tailored for extreme-environment applications.

2 Experimental section

2.1 Preparation of polyimides (PI-6FTB)

NMP was added to a three-neck flask under a nitrogen atmosphere, followed by the dissolution of TFMB under stirring at room temperature for 0.5 h. After complete dissolution, BIA was added, and the mixture was stirred at room temperature for 1 h to ensure homogeneous dispersion. Subsequently,

an equimolar amount of 6FDA was introduced, and the reaction was maintained at 20 °C for 24 h to yield a polyamic acid (PAA) solution with a solid content of 15 wt.%. Thermal imidization was conducted at 200 °C for 6 h using toluene, isoquinoline, and a Dean-Stark trap.

2.2 Preparation of polyimide-Cu complexes (PI-Cu)

PI-Cu50% was used as an example to illustrate the preparation process of coordination networks. First, the PI-6FTB solution (6.67 g, 15 wt.%) was diluted to 8 wt.% with NMP and filtered through a nylon membrane. Separately, copper acetate (0.0524 g, 0.288 mmol) was dissolved in NMP (5 mL) to form a homogeneous $CuAc_2$/NMP solution. The $CuAc_2$/NMP solution was then added dropwise to the diluted PI-6FTB solution under stirring. The mixed solution was cast onto a glass plate and reacted in an oven at 60 °C for 6 h to facilitate coordination. Subsequently, the solvent was evaporated at 80 °C for 24 h, followed by further drying at 250 °C for 12 h, finally yielding dense films with a thickness of 30–40 μm. The pristine PI film was labeled as 6FTB, while the Cu^{2+}-incorporated films were denoted as PI-CuX, where *X* represents the molar ratio of Cu^{2+} to BIA. The synthesis process of PI-6FTB and the PI-Cu films was illustrated in Fig. 1.

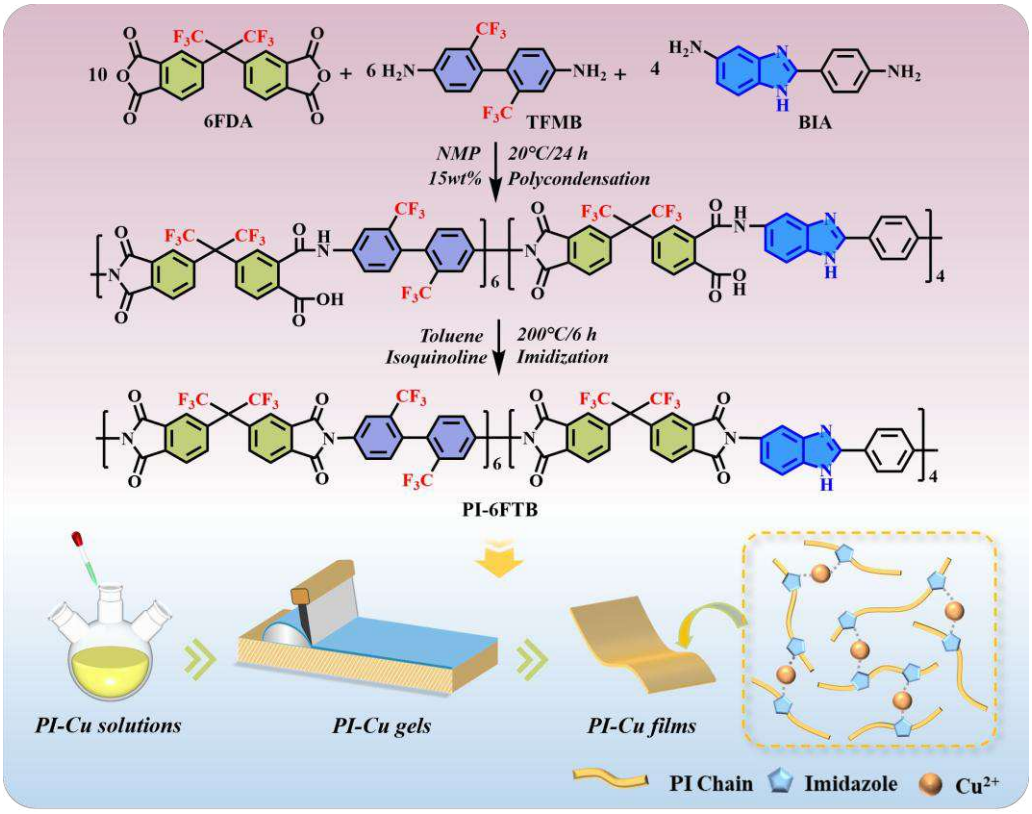


Fig. 1 Synthesis Route of PI-6FTB and PI-Cu Films

3 Results and discussion

3.1 Structural and solution rheology of PI-Cu films

Fig. 2a exhibits the FTIR spectra of the PI-Cu films, which feature characteristic vibrational bands of imide moieties at 1786 cm^{-1} (asymmetric C=O stretching), 1724 cm^{-1} (symmetric C=O stretching), 1366 cm^{-1} (C-N-C stretching), and 718 cm^{-1} (imide ring C=O bending). In addition, the band at 1490 cm^{-1} corresponds to the C=N stretching vibration of the benzimidazole moiety[25]. Notably, the characteristic absorption bands of polyamic acid (PAA) at 1660 cm^{-1} (amide I) and 1550 cm^{-1} (amide II) disappear, confirming a high degree of imidization in the PI-Cu films. Fig. 2b presents the ^1H NMR spectra of PI-Cu films with varying Cu^{2+} contents. The proton resonances at 7.2–8.4 ppm are assigned to aromatic protons in the polyimide backbone. The normalized spectra reveal that as Cu^{2+} content increased, the broadened peaks of the benzimidazole ring gradually disappear, an observation attributed to Cu^{2+} paramagnetism[26]. The characteristic -NH- peak at 13.25 ppm exhibited significant line broadening and intensity reduction. Concurrently, this proton underwent a downfield chemical shift, indicating decreased electron density and weakened shielding in the -NH- group, which further confirms coordination interactions.

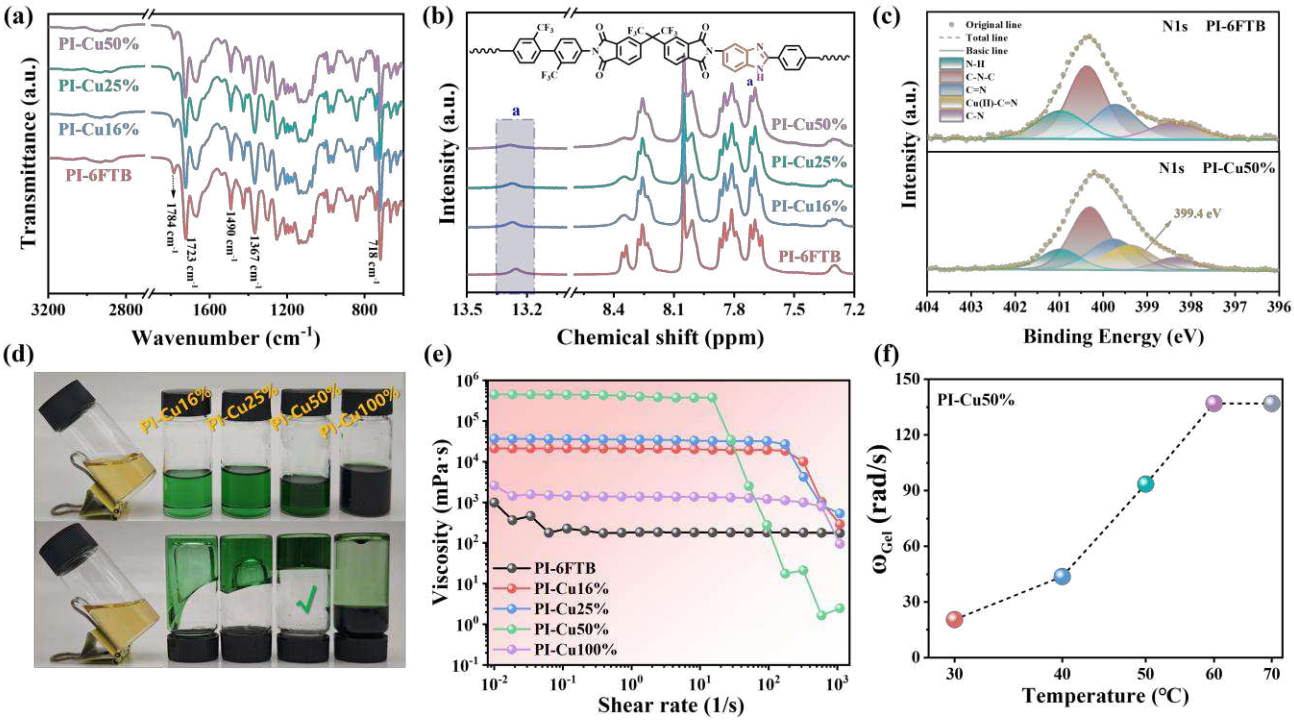


Fig. 2 (**a**) FTIR and (**b**) ^1H NMR spectra of PI-6FTB and PI-Cu films with varying Cu^{2+} contents, (**c**) N 1s XPS spectra of PI-6FTB and PI-Cu50% films, (**d**) digital photographs of PI-Cu coordination complexes, (**e**) apparent viscosity curves of PI-Cu coordination complexes, and (**f**) correlation between the gel point angular frequency

(ω_{Gel}) and temperature for PI-Cu50% coordination complexes

XPS analysis was conducted on PI-Cu films with varying Cu^{2+} contents. As shown in Figs. S1a–b, the PI-Cu films exhibit characteristic core-level peaks at F1s (689.0 eV), O1s (532.0 eV), N1s (400.0 eV), and C1s (284.6 eV). Notably, the PI-Cu films displayed two new peaks at 952.7 eV (Cu $2p_{1/2}$) and 932.5 eV (Cu $2p_{3/2}$). The intensity of these Cu-related peaks increased proportionally with Cu^{2+} loading, confirming the successful integration of Cu^{2+} ions into the polyimide matrix. Fig. 2c presents the N1s spectra, revealing distinct chemical environments: 400.3 eV (sp^3-hybridized C-N-C bonds in imide units), 399.8 eV (C=N bonds in benzimidazole rings), 398.4 eV (C-N bonds in benzimidazole), and 401.0 eV (N-H groups in benzimidazole). A critical observation was the appearance of a new peak at 399.4 eV in the PI-Cu films, attributed to Cu^{2+} coordination with C=N bonds[25]. This coordination-induced spectral shift aligns with the ^{1}HNMR analysis, jointly confirming the C=N→Cu^{2+} coordination structure. These correlated spectral modifications provide direct evidence for the formation of coordination bonds between Cu^{2+} ions and the benzimidazole nitrogen atoms, as predicted by Hard-Soft Acid-Base (HSAB) theory[27]. Furthermore, as shown in Fig. S2, the fluorescence intensity near 500 nm decreased with increasing Cu^{2+} content, exhibiting fluorescence quenching. This was attributed to *d-d* electronic transitions in the Cu^{2+}-benzimidazole complex, confirming the successful formation of the benzimidazole- Cu^{2+} complex within the PI-Cu matrix.

The dissociation-recombination kinetics of metal-ligand coordination was systematically characterized to elucidate how benzimidazole-copper interactions govern solution rheology and to establish precise processing parameters. As illustrated in Fig. 2d, photographs of the PI-Cu solutions revealed a gradual transition to a gel-like, non-flowable state as the Cu^{2+} content increased, which hindered processability. Steady-shear rheometry (Fig. 2e) quantified this trend: apparent viscosity increases by orders of magnitude with Cu^{2+} content, accompanied by progressively pronounced shear-thinning. This nonlinear response typifies dynamic crosslinked networks, where mechanical work at high shear rates overcomes coordination bond energy to induce crosslink dissociation. To confirm the dynamic reversibility of the coordination bonds and the resultant processing feasibility, small-amplitude oscillatory shear rheology was performed on the uncoordinated PI-6FTB and the PI-Cu50% complexes (Fig. S3, strain amplitude 1%, 25 °C). Uncomplexed PI-6FTB maintains liquid-like behavior across 1–100 rad/s, with G'' dominating G'. In contrast, PI-Cu50% exhibits solid-like gel

response ($G' > G''$) at low frequencies, yet undergoes a gel-sol transition at approximately 20 rad/s where G' intersects G''. This transition demonstrates that mechanical energy input at elevated frequencies disrupts the Cu^{2+}-benzimidazole network, enabling solution-based processing.

The temperature sensitivity of the coordination bonds was further investigated through rheological tests. Fig. S4 presents the frequency sweep results of the PI-Cu50% coordination complexes at various temperatures. The gel point angular frequency (ω_{Gel}) was identified as a key parameter for characterizing the dynamic relaxation behavior of the gel network. Elevated temperatures enhanced segmental mobility and accelerated bond dissociation, thereby reducing relaxation times and shifting ω_{Gel} to higher frequencies. The correlation between ω_{Gel} and temperature is shown in Fig. 2f. Notably, ω_{Gel} increased steeply during the initial heating stage, but the rate of increase gradually diminished above 60 °C, eventually approaching a plateau. This plateau indicates that the dependence of the bond exchange rate on temperature weakens, signaling the onset of highly dynamic stable state. The significant variation of ω_{Gel} with temperature directly confirms that the Cu^{2+} coordination bonds exhibit thermally activated dynamic characteristics rather than behaving as static permanent cross-links. Consequently, 60 °C is identified as the optimal processing temperature, providing a critical reference for defining the material's thermal processing window.

3.2 Crosslinking and dynamic characteristics of Metal-coordination bonds

Based on the solution rheology results, 60 °C was identified as the optimal processing temperature. Consequently, a series of composite films with varying Cu^{2+} contents were successfully prepared. As illustrated in Fig. S5, cross-sectional SEM and elemental mapping analyses revealed that PI-6FTB and PI-Cu50% exhibited dense and homogeneous microstructures without pores or cracks. Specifically, elemental mapping validated the uniform distribution of Cu^{2+} across the PI-Cu50% matrix. Furthermore, the excellent consistency between measured and theoretical Cu^{2+} loadings confirmed the effective and uniform integration of Cu^{2+} ions into the polyimide network (Fig. S6).

WAXD was utilized to evaluate variations in chain packing, as presented in Fig. 3a. Both PI-Cu films displayed two broad diffraction peaks located at 13.45° and 29.63°, corresponding to d-spacing values of 6.56 Å and 3.01 Å, respectively, as calculated according to Bragg's law ($2d \sin\theta = n\lambda$, where λ = 1.5406 Å and n=1) [28]. The d_1-spacing value of 6.56 Å is typically interpreted as a measure of

the average intersegmental packing density in amorphous polyimides, reflecting the looseness of chain packing. The smaller d_2-spacing of 3.01 Å is assigned to π-π stacking of aromatic rings[29, 30]. When the Cu^{2+} content was increased to 50%, the d_1-spacing value decreased from 6.56 Å to 6.29 Å, accompanied by a discernible enhancement of the π-π stacking feature. These results indicate that the loosely packed PI chains become tightly packed and the distance between PI chains decreases upon the introduction of Cu^{2+}.

Fig. 3b displays the tanδ curves of the PI-Cu films measured by DMA. The$d$, defined by the tan δ peak maximum, increases monotonically from 386 °C for pristine PI-6FTB to 430 °C for PI-Cu50% with increasing Cu^{2+} content. This upward shift reflects the restriction of cooperative segmental motion by metal-coordination crosslinks[31]. A notable feature is the pronounced broadening of the tan δ peak after crosslinking. This behavior resembles that observed in vitrimers with dynamic covalent bonds and can be understood in similar terms: the thermally activated exchange of coordination bonds introduces a distribution of relaxation times on the experimental timescale, such that different regions of the network undergo their glass transition over a wider temperature range[32]. Concurrently, the peak tanδ intensity decreases with Cu^{2+} content. This reduction indicates diminished energy dissipation during the dynamic exchange process, which can be attributed to two factors. First, the storage modulus at 50 °C, E_1' increases markedly with crosslink density: PI-Cu50% reaches 3.37 GPa compared to only 1.16 GPa for PI-6FTB, a 190% enhancement (Fig. 3c, Table 1). Second, the coordination crosslinks act as physical constraints that reduce the population of chain segments capable of large-scale cooperative motion, thereby lowering internal friction and energy loss during the transition.

Table 1 Thermomechanical Properties of the PI-6FTB and PI-Cu Films

Sample	T_g (℃)	E_1' [a] (GPa)	E_2' [b] (MPa)	*Ve* [c] (mol/m^3)	$T_{d5\%}$ (℃)	T_{dmax} (℃)
PI-6FTB	386	1.16	1.70	99.0	521	591
PI-Cu16%	395	1.04	6.42	368.8	517	555
PI-Cu25%	408	1.93	6.75	380.8	516	550
PI-Cu50%	430	3.37	97.1	5312	512	543

a: Storage modulus of the PI-Cu films at 50℃;
b: Storage modulus of the PI-Cu films at T_g+30℃;
c: *Ve* refers to the crosslinking density.

A further observation concerns the storage modulus behavior above T_g. For the PI-6FTB film, a slight upturn in E′ was detected in the high temperature region, a phenomenon typically attributed to thermal crosslinking induced by partial decomposition[33]. In the PI-Cu coordinated systems, beyond this thermal contribution, the dynamic reorganization of metal-ligand bonds at elevated temperatures likely provides an additional mechanism that reinforces the modulus. To quantitatively evaluate the crosslinked network structure, the crosslink density (V_e) was calculated from the storage modulus E_2' measured at T_g + 30 °C using the rubber elasticity equation V_e = E′/3RT[34]. The results are summarized in Table 1. V_e increased systematically with Cu^{2+} content. Specifically, the V_e value of PI-Cu50% was 53.6 times higher than that of the pristine PI, confirming the effective construction of a dense metal-ligand coordination network and its structural persistence at high temperatures. TGA data are presented in Fig. S7 and summarized in Table 1, reveal that both $T_{d5\%}$ and T_{dmax} decreased progressively with Cu^{2+} incorporation, consistent with the well-documented catalytic effect of metal ions on polymer degradation[35]. Despite this trend, all the samples exhibited excellent thermal stability below 500 °C, with no significant weight loss observed in this temperature range.

Room-temperature tensile tests (Figs. 3d–e) reveal that Cu^{2+} coordination markedly stiffens and strengthens the PI-Cu films: Young's modulus rises from 3.3 GPa (PI-6FTB) to 4.4 GPa (PI-Cu50%, +33.3%), and tensile strength from 95 MPa to 128 MPa (+34.7%), while elongation at break declines monotonically with crosslink density. This embrittlement reflects a fundamental shift in deformation mechanism. PI-6FTB yields and softens beyond ~5% strain, whereas PI-Cu films fracture before yielding, indicating that Cu^{2+}–benzimidazole cross-links effectively arrest segmental slip and hinder molecular orientation. These mechanical signatures confirm that the coordination network behaves as a “quasi-static” cross-linked system at ambient temperature. Theoretically, "quasi-static" cross-linking characteristics increase the proportion of elastic deformation, thereby enhancing the room-temperature storage modulus, elastic modulus, and cyclic stability under small strains[36]. On this basis, cyclic tensile tests were conducted (Fig. 3f). The residual strain of PI-Cu50% at 4% strain is only 0.47%, which is significantly lower than the 1.38% observed for PI-6FTB. After 20 cycles, the tensile strength retention rate of PI-Cu50% reaches 93.8%, whereas the PI-6FTB exhibits a strength loss of 26.4%. Meanwhile, in the room-temperature creep test shown in Fig. S8, the creep recovery rate of PI-Cu50% approached 99.4% (94.1% for PI-6FTB), indicating that the unbroken or recombined coordination

bonds effectively drive chain retraction and provide recoverable entropic elastic restoring forces. These results further confirm the effective suppression of irreversible deformation accumulation by the "quasi-static" coordination cross-linking network.

When the temperature enters the dynamic activation regime, the coordination cross-linked network undergoes reversible topological rearrangement while preserving its integrity. Temperature-dependent tensile tests revealed a unique transition in the mechanical behavior of PI-Cu50%. At 150 °C, PI-Cu50% still exhibits higher strength and modulus than PI-6FTB but a lower elongation at break, consistent with the room-temperature trend, indicating that the coordination bonds remain largely “quasi-static” cross-linked and impose rigid constraints (Fig. 3g). At 200 °C, the elongation at break of PI-Cu50% (55%) significantly surpassed that of PI-6FTB (17%), while the former continues to retain higher strength and modulus, achieving a synergy of strength and toughness . This transition suggests that the evolution from a "quasi-static" constraint to a thermally activated dynamic regime, as illustrated in the schematic in Fig. 3h. Elevated temperatures accelerate the dissociation-reassociation kinetics of the coordination bonds. Bond dissociation provides additional degrees of freedom for chain slippage during stretching; the dissociated chains subsequently re-coordinate at new sites following orientation and rearrangement. This "dissociation-slip-reassociation" cycle transforms the deformation mechanism from brittle fracture to ductile stretching, thereby substantially enhancing elongation at break. Similar behavior has been observed in vitrimers[37], where dynamic bonds enable stress relaxation via bond exchange, delaying crack propagation and suppressing chain scission, thus achieving higher elongation at break without sacrificing strength.

Upon further heating to 300 °C, the ligand exchange intensifies, yet the network remains effectively cross-linked, as evidenced by the highest storage modulus in Fig. 3c. Transient dissociation of the coordination bonds reduces the effective crosslink density, leading to slightly lower strength, modulus, and elongation at break compared to 200 °C. High-temperature stress relaxation measurements (Fig. S9) were conducted to probe the efficacy of coordination bonds at elevated temperatures. The characteristic relaxation times (τ) of both materials decrease with temperature, consistent with thermally activated segmental motion. Notably, PI-Cu50% exhibits a larger τ than PI-6FTB at all temperatures, and its temperature dependence is considerably weaker: τ decreases by a factor of ~6 for PI-Cu50% versus ~19 for PI-6FTB. This result suggests that, even when the

coordination bonds become dynamic at high temperatures, their rapid re-association sustains a sufficiently high effective crosslink density during the dissociation–reassociation cycles, thereby suppressing irreversible chain slip and macroscopic relaxation. Furthermore, such a network benefits dimensional stability: the CTE of PI-Cu50% is 35.92 ppm/K, lower than 40.17 ppm/K for PI-6FTB (Fig. S10).

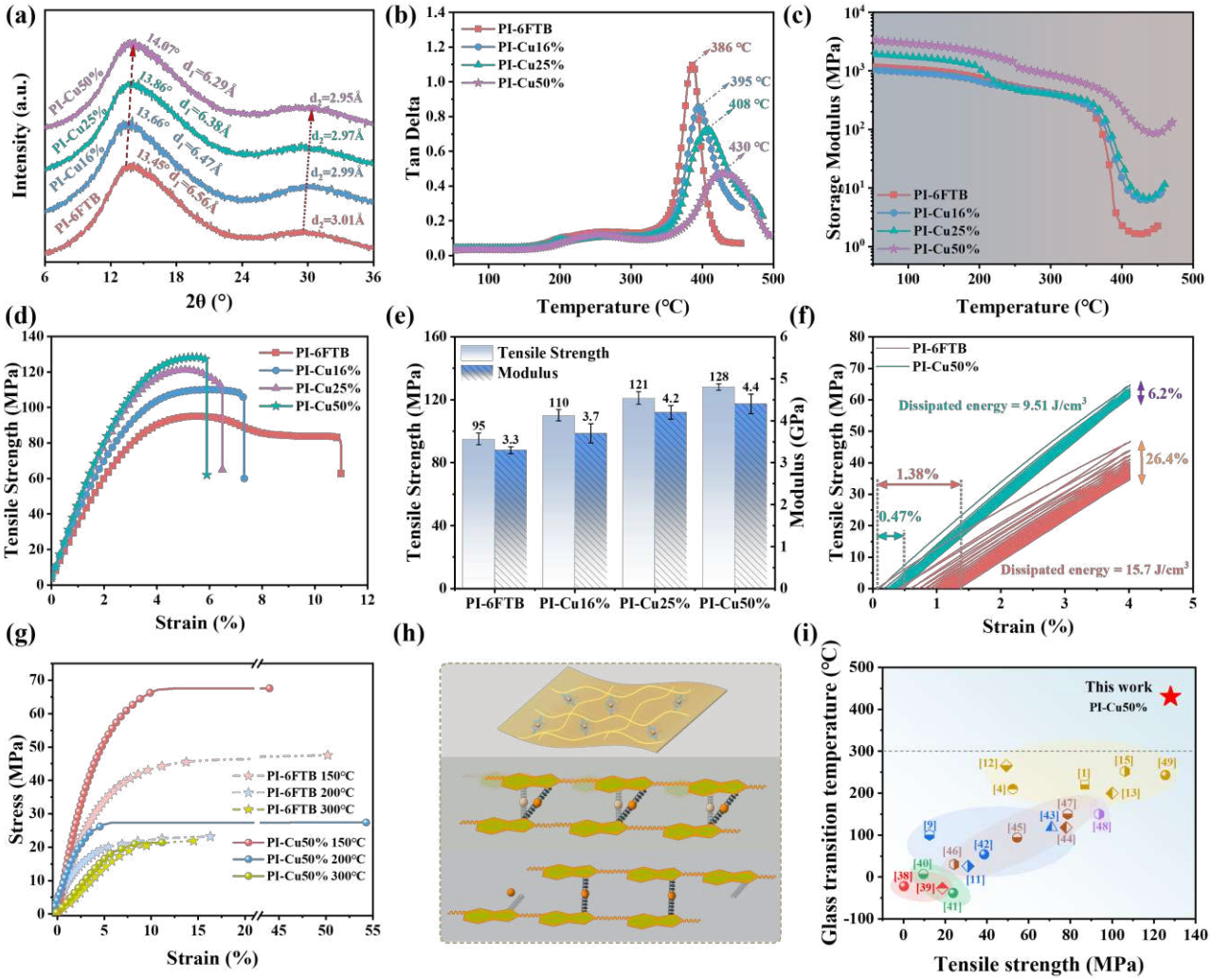


Fig. 3 Mechanical and thermomechanical properties of PI-6FTB and PI-Cu films. (**a**) XRD patterns of PI-Cu films with varying Cu^{2+} contents, (**b**) temperature-dependent tanδ, (**c**) storage modulus as a function of Cu^{2+} contents, (**d**) tensile stress-strain curves, (**e**) histogram summarizing the mechanical properties, (**f**) repeated cyclic tensile curves of PI-6FTB and PI-Cu50% films at a fixed strain of 4%, (**g**) stress-strain curves of PI-6FTB and PI-Cu50% films at different temperatures, (**h**) schematic illustration of the coordination mechanism in PI-Cu films under cyclic stress, and (**i**) comparison of tensile strength and glass transition temperature of dynamically recycled polymers. Red, green, blue, brown, purple, and yellow symbols denote polyester[38, 39], polyolefin[40, 41], polyurethane[9, 11, 42, 43], epoxy[44-47], polyether ether ketone[48], and polyimide[1, 4, 12, 13, 15, 49], respectively

Collectively, the Cu^{2+}–benzimidazole coordination crosslinking constructs a unique dynamic

network over a wide temperature range: at room temperature, it exhibits a "quasi-static" crosslinking characteristic, significantly enhancing modulus, strength, and cyclic stability; at elevated temperatures, the thermally activated dynamic exchange of coordination bonds endows the network with stress dissipation and topological rearrangement capabilities, suppressing macroscopic relaxation and thermal expansion while maintaining a relatively high effective crosslink density. To the best of our knowledge, PI-Cu50% exhibits the highest T_g (430 °C) reported to date for a dynamic cross-linked polymer, while its tensile strength ranks among the highest values documented for such systems, as shown in the comparative summary of representative dynamic polymer networks in Fig. 3i.

3.3 Bending and fatigue resistance properties of PI-Cu films

In demanding applications such as flexible electronics and high-temperature electrical insulation, polymer films are subjected to repeated bending, imposing stringent requirements on fatigue resistance and structural integrity. The above analyses show that the “quasi-static” coordination cross-links in PI-Cu50% effectively suppress irreversible segmental slip, resulting in superior fatigue resistance. We further examined the durability of PI-6FTB and PI-Cu50%. Fig. 4a illustrates a schematic of the PI-Cu film bending test. In this setup, the bending radius between the two plates was fixed at 2 mm, and a full bending cycle was defined as the transition of the plates from fully closed (0°) to fully open (180°). The PI-6FTB and PI-Cu50% films were subjected to 50k, 100k, 200k, and 400k preset bending cycles, respectively. Fig. S11a presents SEM images of the PI-6FTB film in its pristine state and after 50k bending cycles (showing both inner and outer surfaces). Evident deep cracks were observed, indicating severe structural damage. Notably, this film fractured at 100k cycles, with SEM images of its fracture cross-section and optical photos of its fracture morphology shown in Fig. S11b.

By contrast, no obvious creases or cracks were observed with the naked eye on the PI-Cu50% film after 400k bending cycles (as shown within the red box in Fig. 4b (I)). Analysis of the stress-strain curves of the PI-Cu50% film after different bending cycles revealed that the tensile strength retention rate (≥ 83.3%) and elongation at break retention rate (≥ 90.7%) remained at high levels, as shown in Fig. 4c. To further explore the microstructure, SEM characterization was performed on the inner and outer surfaces of the PI-Cu50% film after 400k bending cycles (Fig. S11c). The results show only partial scratches on the film surface with no obvious cracks, further verifying its excellent bending resistance. These findings lay a theoretical and technological foundation for the application of such

materials in next-generation flexible optoelectronics manufacturing.

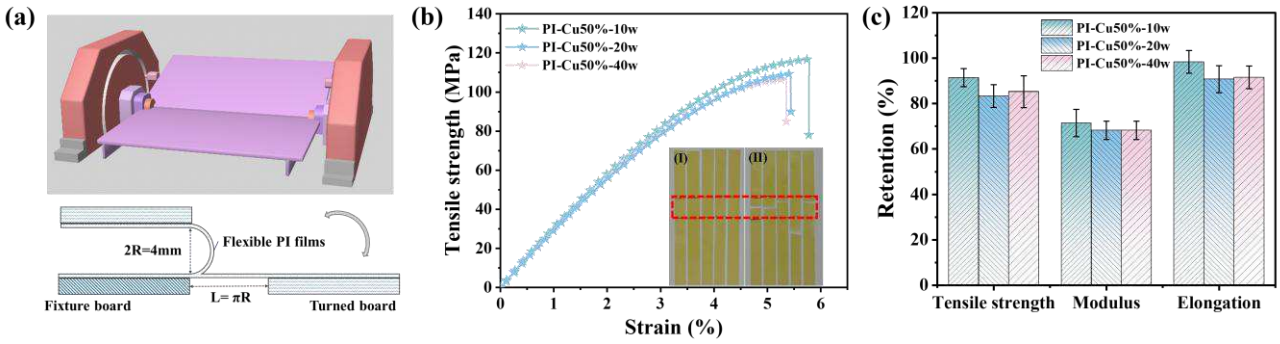


Fig. 4 Bending stability and mechanical durability of PI-Cu50% film. (**a**) Bending schematic diagram, (**b**) stress-strain curves under different bending cycles and optical photos before and after 400,000 bending cycles, and (**c**) mechanical properties retention rates after different bending cycles

3.3 Dielectric properties of PI-Cu films

The dielectric properties of PI-Cu films are displayed in Fig. 5, which shows that the introduction of Cu^{2+} effectively enhances the dielectric stability of the PI-Cu film. Fig. 5a illustrates the dielectric constant of PI-Cu films measured at room temperature. With the Cu^{2+} content increased, the dielectric constant (ε') at 1 kHz exhibits a marked increase from 3.04 to 4.13, as the introduced Cu^{2+} provides more ion polarization[50, 51]. Simultaneously, the lone electron pairs of the imidazole units form *d*-π bonds with the empty *d* orbitals of Cu^{2+}, inducing long-range electron delocalization within the conjugated system and thereby increasing the molecular dipole moment[52, 53]. These two factors act synergistically to elevate the dielectric constant of the PI-Cu films.

Although Cu^{2+} introduction is typically expected to increase ionic conduction loss, the dielectric loss of the PI-Cu films exhibits a systematic decreasing with increasing Cu^{2+} content, significantly dropping from 0.014 to 0.012 at 1 kHz (Fig. 5b). This decrease is primarily attributed to the sustained constraint imposed by the coordination crosslinked network on long-range segmental motion, which restricts the rotational relaxation of polymer chain segments and the orientation of polar groups (e.g., $–CF_3$, C=O), thereby effectively suppressing segmental relaxation loss. Breakdown strength is a core metric for assessing the insulation reliability of dielectric materials. The PI-Cu50% film exhibits a combination of high dielectric constant and low dielectric loss over a broad frequency range, establishing a favorable basis for enhanced breakdown strength. As shown in Fig. 5c, the breakdown strength was significantly enhanced with the increasing Cu^{2+} content from an initial 392 MV/m to 514

MV/m, representing a relative improvement of 31.1%. This performance enhancement is attributed to the formation of a coordination cross-linked network, which enhances chain packing and reduces free volume, thereby minimizing charge carrier mobility and suppressing the formation of conductive pathways. Consequently, constructing a Cu^{2+}–benzimidazole coordination network simultaneously enhances microscopic polarization and suppresses mesoscopic relaxation, leading to overall improved dielectric performance.

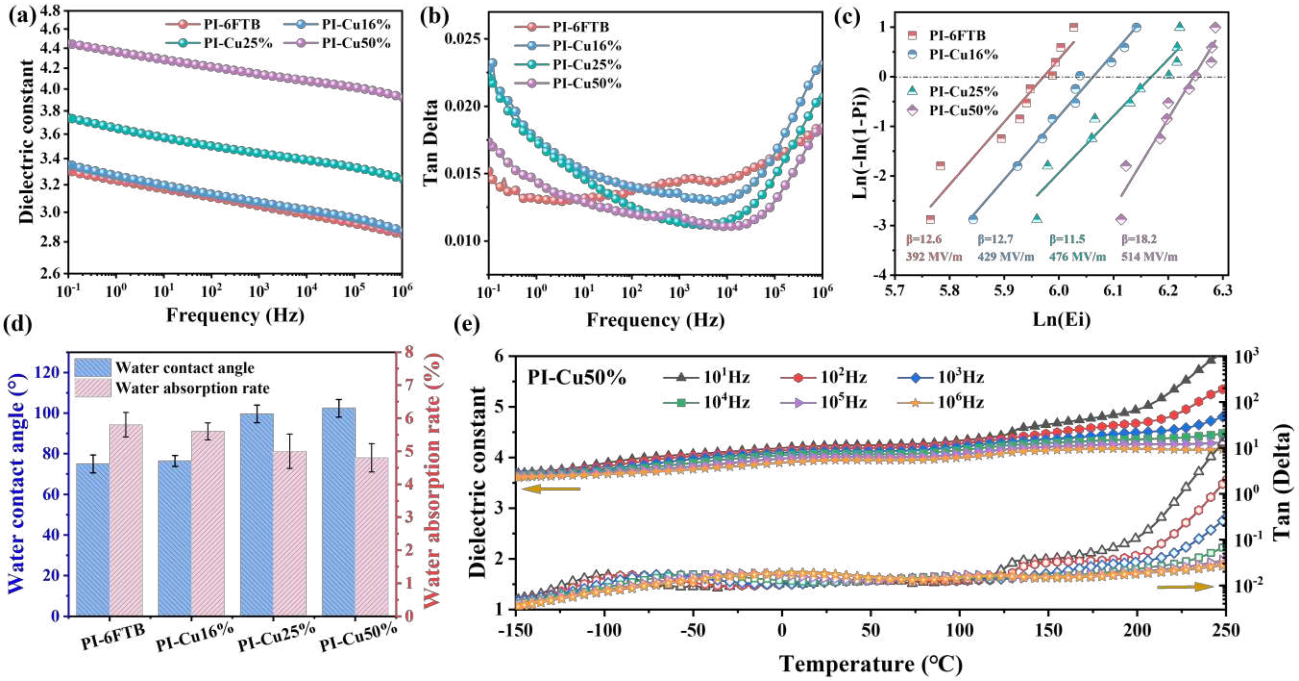


Fig. 5 Dielectric properties and water resistance of PI-6FTB and PI-Cu films. (**a**) Dielectric constant (ε'), (**b**) dielectric loss tangent (tanδ) as a function of frequency, (**c**) electrical breakdown strength, (**d**) water contact angle and water absorption rate, (**e**) temperature-dependent dielectric constant and tanδ of PI-Cu50% film

For the increasingly severe thermo-electric coupling stress challenge faced by high-power flexible electronic devices, dielectric materials must maintain a stable dielectric response over a wide temperature range to ensure operational reliability under extreme conditions[54]. Moisture typically degrades dielectric performance by enhancing polarization losses or introducing additional relaxation processes[55]. To address this, the water uptake behavior of PI-6FTB and PI-Cu films was evaluated. Owing to the occupation of the lone-pair electrons on the imidazole nitrogen by Cu^{2+}, along with the dense chain packing, the PI-Cu film exhibits a low water uptake (Fig. 5d), rendering it less susceptible to moisture interference during practical use[56]. This lays the foundation for achieving dielectric stability over a broad temperature range.

Fig. S12 and Fig. 5e illustrate the temperature-dependent dielectric properties of the PI-6FTB and PI-Cu50% films. In comparison with analogous work reported in the literature, the PI-Cu50% film exhibits excellent temperature stability in its dielectric properties[57]. Specifically, the temperature coefficient of the dielectric constant, which quantitatively describes the rate of change of the dielectric constant with increasing temperature, is determined using the following equation[58]:

$$\tau_\varepsilon = \frac{\varepsilon_f - \varepsilon_i}{\varepsilon_r\,(T_f - T_i)}$$

where τ_ε is the temperature coefficient of dielectric constant, ε_f, ε_i, and ε_r are the dielectric constant at final temperature, initial temperature, and room temperature respectively, T_f and T_i are the final temperature and initial temperature.

Considering the interference of electrode polarization on the dielectric response at high temperatures and low frequencies (>200 °C, <10 Hz) [59], the temperature coefficient was calculated only for the frequency range of 100 Hz to 1 MHz, as shown in Fig. S13. The crosslinked PI-Cu50% film exhibits excellent thermal stability, with a τ_ε value of 6.9×10^{-4} °C^{-1} at 1 kHz and 250 °C, which is significantly lower than that of the PI-6FTB film. This value is comparable to (or even lower than) that of the crosslinked polyarylene ether nitrile film reported[58].

3.4 Solvent resistance and recyclability properties of PI-Cu films

Solvent resistance is a critical metric for evaluating the service reliability of polymeric films in complex chemical environments, and is particularly important for electronic device encapsulation and flexible substrate applications that involve exposure to organic solvents or wet processing. To assess the effect of Cu^{2+} coordination crosslinking on the solvent resistance, the PI-6FTB and PI-Cu50% films were sequentially immersed into chloroform, ethyl acetate, acetone, THF, DMAc, NMP and DMSO for 20 minutes and 24 hours at ambient temperature, as shown in Fig. S14. PI-6FTB underwent rapid dissolution in polar aprotic solvents and disintegrated completely within 20 minutes in acetone, THF, DMAc, NMP and DMSO. In stark contrast, PI-Cu50% exhibited exceptional stability, maintaining structural integrity in all solvents even after 24 hours of immersion. Table S1 summarizes the solubility properties of PI-6FTB and PI-Cu50% films. Furthermore, gel fraction analysis was used to quantify crosslinking. As shown in Figs. 6a-b, PI-Cu50% retained >86% gel content in NMP at 25 °C after 24 h, whereas PI-6FTB rapidly dissolved, precluding measurement after 20 min.

The excellent solvent resistance of PI-Cu50% is attributed to the enhancement of interchain interactions by the "quasi-static" coordination crosslinking network. The crosslinking points effectively hinder solvent penetration and chain segment leaching, endowing the system with the core advantages of both thermoplastic and thermoset polyimides: it allows for solution processing, while the crosslinked material exhibits outstanding thermal stability, mechanical properties, and solvent resistance.

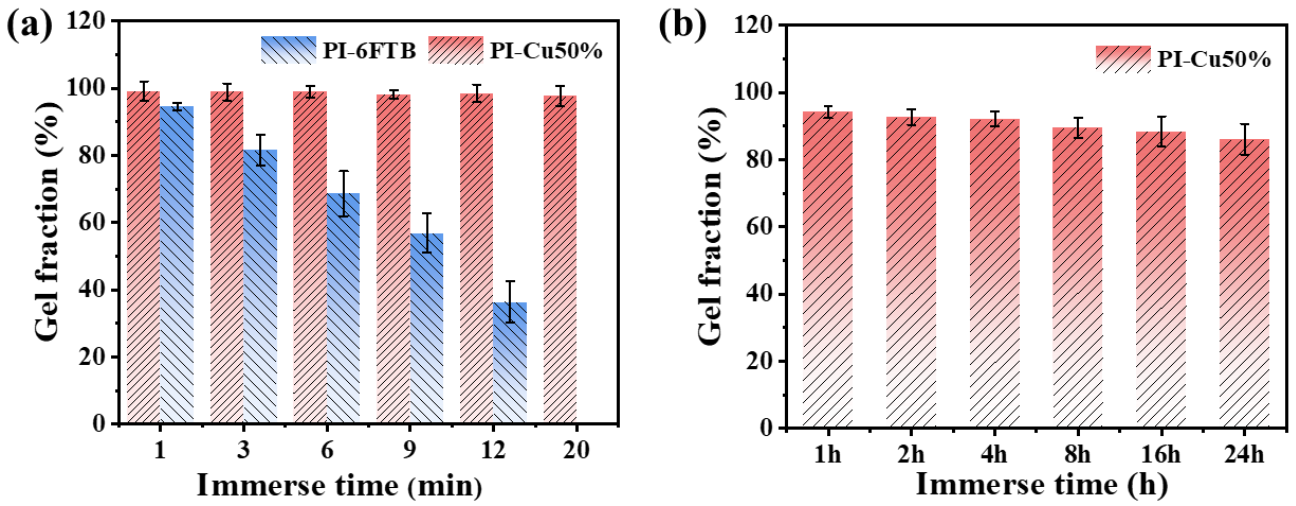


Fig. 6 Solvent resistance and gel fraction analysis. (**a**)-(**b**) Gel fraction of PI-6FTB and PI-Cu50% fil ms after immersion in NMP

However, this "quasi-static" crosslinking network can undergo directed dissociation via competitive ligands, enabling closed-loop recycling of the material. As a hexadentate ligand, EDTA exhibits exceptional chelating capability toward metal ions. Density functional theory (DFT) calculations revealed that the binding energy of the EDTA-Cu^{2+} system (ΔE = -3853.64 kJ/mol) is significantly higher than that of the benzimidazole-Cu^{2+} system (ΔE = -1526.87 kJ/mol), corresponding to an approximately 152% enhancement in binding energy, as shown in Fig. 7b. This thermodynamic evidence confirms EDTA's superior coordination stability with Cu^{2+}, providing a theoretical foundation for the subsequent dynamic dissociation and recovery of PI-Cu cross-linked films. Most importantly, bulky trifluoromethyl (CF_3) groups were introduced near the coordination centers. These side groups created sufficient free volume for segmental motion, which facilitated the penetration of EDTA molecules and promoted the dynamic dissociation and recombination of coordination bonds.

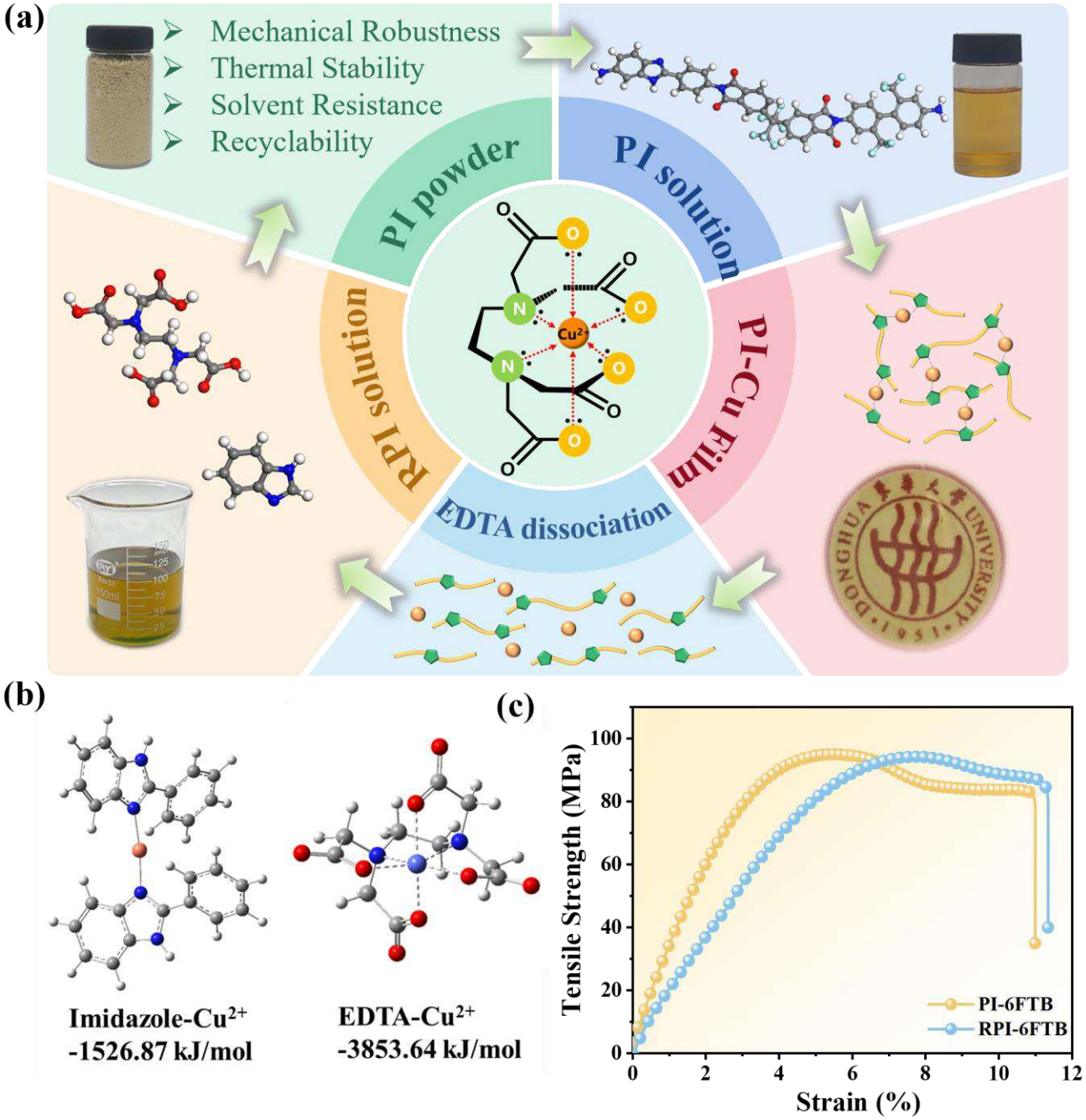


Fig. 7 Recovery process of PI-6FTB. (**a**) Schematic illustration of the PI-6FTB recovery process, (**b**) 3D conformation and binding energy simulation of Cu^{2+} coordination structure, and (**c**) stress-strain curves of PI-6FTB and RPI-6FTB films

NMP was used to swell the PI-Cu films to promote the entry of EDTA molecules, which possess stronger coordination ability, into the coordination sites, thereby realizing the dissociation of metal coordination bonds. Notably, the PI-Cu50% film completely dissolved in a saturated EDTA/NMP mixed solvent within 8 hours. Fig. 7a illustrates the closed-loop recycling process for recovering PI-6FTB from PI-Cu50%. After separating the EDTA-Cu^{2+} complex via centrifugation, the PI solution

was dropwise precipitated in absolute ethanol, followed by thorough washing and drying. This procedure successfully yielded linear PI-6FTB with a recovery rate of ≥ 91%. The recovered polymer was subsequently re-cast using the original fabrication protocol to obtain regenerated films, designated as RPI-6FTB.

As shown in Fig. S15, RPI-6FTB was characterized by FTIR, ^{1}HNMR, and DMA. RPI-6FTB retained intact characteristic peaks of polyimide, and its T_g remained virtually identical to that of the pristine polymer, confirming a non-destructive recovery process. Furthermore, the mechanical properties of RPI-6FTB were evaluated by tensile testing, as shown in Fig. 7c. Analysis of the stress-strain curves revealed a tensile strength of 94.2 MPa for the RPI-6FTB, representing a 99.2% retention compared to the pristine sample. These results demonstrate the excellent recyclability of the PI-Cu50% film. This coordination crosslinking strategy overcomes the bottleneck of reconciling "high stability" with "recyclability" in traditional high-performance polymers, endowing the material with post-consumer recyclability while maintaining its service capability in extreme environments.

4 Conclusions

This study presents a high-performance, recyclable polyimide material (PI-Cu) constructed by incorporating benzimidazole units into a rigid aromatic backbone with Cu^{2+} ions, giving rise to a “quasi-static” coordination cross-linked network. This strategy reconciles the long-standing conflict between thermal stability, mechanical properties, and recyclability. The optimized PI-Cu50% film achieves a glass transition temperature of 430 °C, a tensile strength of 128 MPa and a Young's modulus of 4.4 GPa. To the best of our knowledge, these are the highest reported values for a dynamic polymer network. It also exhibits exceptional fatigue resistance with a residual strain below 0.5% after 20 stretching cycles. Moreover, it maintains a stable dielectric constant and low dielectric loss across the −150 to 250 °C range, with a breakdown strength reaching 514 MV/m. At 200 °C, the network switches into a dynamic regime while retaining higher strength and modulus than PI-6FTB. Meanwhile, its elongation at break surges to over three times that of PI-6FTB, achieving a synergy of strength and toughness at elevated temperature. Despite its excellent solvent resistance, PI-Cu50% can be fully depolymerized via mild EDTA treatment, and the recovered film retains more than 99% of its original tensile strength. This work leverages strong yet dynamic coordination bonds to resolve the inherent conflict among rigidity, high performance, and recyclability, achieving a transition from "rigid

confinement" at room temperature to "dynamic adaptation" at elevated temperatures. This strategy provides a new route to sustainable, high-performance polymers for extreme conditions, with promising applications in fields such as deep-space exploration and soft robotics.

Funding

This work was supported by the Fundamental Research Funds for the Central Universities (No. 2232025G-12-1 and No. CUSF-DH-T-2024007).

Data availability

No datasets were generated or analysed during the current study.

References

1. Wan B, Zheng MS, Yang X, Dong X, Li Y, Mai YW, Chen G, Zha JW (2023) Recyclability and Self-Healing of Dynamic Cross-Linked Polyimide with Mechanical/Electrical Damage. Energy Environ Mater 6(1):e12427. https://10.1002/eem2.12427

2. Dong J, Hu R, Xu X, Chen J, Niu Y, Wang F, Hao J, Wu K, Wang Q, Wang H (2021) A Facile In Situ Surface-Functionalization Approach to Scalable Laminated High-Temperature Polymer Dielectrics with Ultrahigh Capacitive Performance. Adv Funct Mater 31(32):2102644. https://10.1002/adfm.202102644

3. Wang X, Gao FL, Zhao HY, Tian L, Li S, Wang S, Yu ZZ, Li X (2025) Polymer-Based Dielectric Composite Films with Excellent Dielectric Energy Storage and Thermal Management Capabilities. Adv Funct Mater 36(3):e12371. https://10.1002/adfm.202512371

4. Wan B, Xiao M, Dong X, Yang X, Zheng MS, Dang ZM, Chen G, Zha JW (2023) Dynamic Covalent Adaptable Polyimide Hybrid Dielectric Films with Superior Recyclability. Adv Mater 36(52):2304175. https://10.1002/adma.202304175

5. Li F, Wang Y, Li J, Xie H, Wang J (2025) Soluble, colorless and biobased polyimides with high thermal stability derived from renewable anethole. J Mater Chem C 13(25):12783–12792. https://10.1039/d5tc01284h

6. Wang B, Ma S, Yan S, Zhu J (2019) Readily recyclable carbon fiber reinforced composites based

on degradable thermosets: a review. Green Chem 21(21):5781-5796. https://10.1039/c9gc01760g

7. Peng Z, Zhang L, Li C (2025) Low dielectric and high thermal conductivity polyimide nanocomposites with fully closed-loop recycling and highly consistent healing. Compos B Eng 299:112390. https://10.1016/j.compositesb.2025.112390

8. DAMIEN MONTARNAL M C, FRANÇOIS TOURNILHAC, AND LUDWIK LEIBLER (2011) Silica-Like Malleable Materials from Permanent Organic Networks. Science 334(6058):965-968. https://10.1126/science.1212648

9. Tan P, Zhao X, Zhang Z, Wei W, Zhou J, Shao Y, Ma X, Wei S, Gao Z, Han S (2024) A Highly Effective Self-Healing Waterborne Polyurethane Vitrimer Containing Conjugated Schiff Base Bonds Driven by Photothermal. ACS Appl Polym Mater 6(15):8977-8988. https://10.1021/acsapm.4c01274

10. Liu W, Wang X, Chen Y (2024) Fully Recycled Polyolefin Elastomer-Based Vitrimers with Ultra-High, Universal, Stable, and Switchable Adhesion. Small 20(44):2403934. https://10.1002/smll.202403934

11. Huyan C, Liu D, Pan C, Wang D, Guo Z, Zhang X, Dai S, Bin Xu B, Chen F (2023) Thermally recyclable and reprocessable glass fiber reinforced high performance thermosetting polyurethane vitrimer composites. Chem Eng J 471:144478. https://10.1016/j.cej.2023.144478

12. Li F, Yu P, Wu B, Cao M, Xia R, Qian J (2026) Dual-dynamic polyimide and its thermally conductive adhesive featuring high glass transition temperature, recyclability, and strong adhesion. Chem Eng J 528:172195. https://10.1016/j.cej.2025.172195

13. Wan B, Yang X, Dong X, Zheng MS, Zhao Q, Zhang H, Chen G, Zha JW (2022) Dynamic Sustainable Polyimide Film Combining Hardness with Softness via a “Mimosa-Like” Bionic Strategy. Adv Mater 35(2):2207451. https://10.1002/adma.202207451

14. Luo C, Wang W, Yang W, Liu X, Lin J, Zhang L, He S (2023) High-Strength and Multi-Recyclable Epoxy Vitrimer Containing Dual-Dynamic Covalent Bonds Based on the Disulfide and Imine Bond Metathesis. ACS Sustainable Chem Eng 11(39):14591-14600. https://10.1021/acssuschemeng.3c04345

15. Wan B, Liu H, Wang J, Xing Y, Gao J, Jung Y C, Zha JW (2025) Self-healing and recyclable polyimide hybrid film with linear and crosslinked bridging structure. Compos B Eng 306:112769. https://10.1016/j.compositesb.2025.112769

16. Mahmoodi R, Zabihi O, Zamani M R, Ahmadi M, Laghaei M, Zamani P, Ferdowsi M R G, Zohuriaan-Mehr M J, Naebe M (2025) Zero-waste closed-loop recycling of carbon fiber reinforced vitrimer-based polymer composites with a long-extended prepreg shelf life. Advanced Composites and Hybrid Materials 8(5):369. https://10.1007/s42114-025-01463-2

17. Yenpech N, Chirachanchai S (2025) Mechanochromic Building Blocks with a Dynamic Chemical Cross-Linking Network in Shape Memory Polycaprolactone: A Model Strategy for Integrating Reversibility, Repeatability, and Recoverability into a Single Multiresponsive Material. ACS Sustainable Chem Eng 13(42):17991-18005. https://10.1021/acssuschemeng.5c06610

18. Zhou Q, Gardea F, Sang Z, Lee S, Pharr M, Sukhishvili S A (2020) A Tailorable Family of Elastomeric-to-Rigid, 3D Printable, Interbonding Polymer Networks. Adv Funct Mater 30(30):2002374. https://10.1002/adfm.202002374

19. Peter T. Corbett, Julien Leclaire, Laurent Vial, Kevin R. West, Jean-Luc Wietor, Jeremy K. M. Sanders, Otto a (2006) Dynamic Combinatorial Chemistry. Chem Rev 106(9):3652–3711. https://10.1021/cr020452p

20. Li C H, Zuo J L (2019) Self-Healing Polymers Based on Coordination Bonds. Adv Mater 32(27):1903762. https://10.1002/adma.201903762

21. Yu X, Fu Z, Wang K, Guo X, Lu Y, Yao L (2026) Metal-polyphenol networks facilitate the construction of recyclable fiberboard. Advanced Composites and Hybrid Materials 9(2):196. https://10.1007/s42114-026-01753-3

22. Zhou X, Jin B, Zhu Z, Wu J, Zhao Q, Chen G (2024) Metal-Ligand Bonds Based Reprogrammable and Re-Processable Supramolecular Liquid Crystal Elastomer Network. Angew Chem Int Ed 63(44):e202409182. https://10.1002/anie.202409182

23. Zhao ZH, Chen SY, Zhao PC, Luo WL, Luo YL, Zuo JL, Li CH (2024) Mechanically Adaptive Polymers Constructed from Dynamic Coordination Equilibria. Angew Chem Int Ed 63(17):e202400758. https://10.1002/anie.202400758

24. Jiang S, Bi Z, Wang J, Zhao J, Fan L, Tian L, Wu Y, Yi N, Wei Z, Gan F (2023) Construction of novel Cu-α-diimide interactions for enhancing thermal resistance and dimensional stability of polyimide films. J Mater Res Technol 25:1920-1930. https://10.1016/j.jmrt.2023.06.064

25. Gan F, Wang J, Wen J, Zhou J, Mo J, Han S, Wu Y, Yi N (2022) Preparation of polyimide-metal

complexes with tunable Sol-Gel transition by Introduction of Zn(II)-Coordination. Polym Test 111:107615. https://10.1016/j.polymertesting.2022.107615

26. Novotny J, Komorovsky S, Marek R (2024) Paramagnetic Effects in NMR Spectroscopy of Transition-Metal Complexes: Principles and Chemical Concepts. Acc Chem Res 57(10):1467-1477. https://10.1021/acs.accounts.3c00786

27. Giancaspro M, Sibillano T, Panzarea F, Giannini C, Schmitzer S, Vischio F, Depalo N, Agostiano A, Curri ML, Striccoli M, Fanizza E (2021) $Cu_{2-x}S$ nanocrystal synthesis: a chemical toolbox for controlling nanocrystal geometry, phase and plasmonic behavior. Mater Chem Front 5(3):1341-1354. https://10.1039/d0qm00596g

28. Ahn C, Kim TY, Hong PH, Choi S, Lee YJ, Kwon H, Jeon H, Ko DW, Park I, Han H, Hong SW (2022) Highly Transparent, Colorless Optical Film with Outstanding Mechanical Strength and Folding Reliability Using Mismatched Charge-Transfer Complex Intensification. Adv Funct Mater 32(20):2111040. https://10.1002/adfm.202111040

29. Shi Y, Liang J, Babu Shrestha B, Wang Z, Zhang Y, Jin J (2022) Enhancing the CO_2 plasticization resistance of thin polymeric membranes by designing Metal-polymer complexes. Sep Purif Technol 289:120699. https://10.1016/j.seppur.2022.120699

30. Liang J, Wang Z, Huang M, Wu S, Shi Y, Zhang Y, Jin J (2020) Effects on Carbon Molecular Sieve Membrane Properties for a Precursor Polyimide with Simultaneous Flatness and Contortion in the Repeat Unit. ChemSusChem 13(20):5531-5538. https://10.1002/cssc.202001572

31. Guo X, Nakagawa S, Yoshie N (2024) Tunable Mechanical Properties in Microphase-Separated Thermoplastic Elastomers via Metal–Ligand Coordination. Macromolecules 57(5):2351-2362. https://10.1021/acs.macromol.4c00178

32. Capelot M, Unterlass MM, Tournilhac F, Leibler L (2012) Catalytic Control of the Vitrimer Glass Transition. ACS Macro Letters 1(7):789-792. https://10.1021/mz300239f

33. Luo F, Zhao J, Jiao L, Du Z, Dong Z, Zhang Y, Sun Z, Qiu X (2024) Preparation and properties of high temperature colorless transparent polyimide containing semi-alicyclic and bisbenzoxazole structure. Polymer 315:127787. https://10.1016/j.polymer.2024.127787

34. Li B, Zhu G, Hao Y, Ren T (2024) Effect of cross-link density on the performance of polyimine/epoxy vitrimers. Smart Mater Struct 33(2):025014 -025022. https://10.1088/1361-

665X/ad1c54

35. Zhan L, Wu L, Tian G, Wu H, Tian G, Qi S, Wu D (2020) Effect of Metal Ion Loading on Thermal Decomposition Temperature of Surface Modified Polyimide Films. J Funct Polym 33(5):467-472. https://10.14133/j.cnki.1008-9357.20191119001

36. Park K, Mishra S, Lewis G, Losby J, Fan Z, Park JB (2004) Quasi-static and dynamic nanoindentation studies on highly crosslinked ultra-high-molecular-weight polyethylene. Biomaterials 25(12):2427-2436. https://10.1016/j.biomaterials.2003.09.014

37. Pandya H, Khabaz F (2024) Effect of dynamic bond concentration on the mechanical properties of vitrimers. Chem Commun 60(75):10354-10357. https://10.1039/d4cc03030c

38. Yue L, Su YL, Li M, Yu L, Montgomery S M, Sun X, Finn M G, Gutekunst W R, Ramprasad R, Qi H J (2023) One-Pot Synthesis of Depolymerizable δ-Lactone Based Vitrimers. Adv Mater 35(29):2300954. https://10.1002/adma.202300954

39. Zheng J, Lu J, Yang Z, Liu T (2024) Fabrication of recyclable and biodegradable PBAT vitrimer via construction of highly dynamic cross-linked network. Polym Degrad Stab 219:110602. https://10.1016/j.polymdegradstab.2023.110602

40. Chen Y, Tang Z, Liu Y, Wu S, Guo B (2019) Mechanically Robust, Self-Healable, and Reprocessable Elastomers Enabled by Dynamic Dual Cross-Links. Macromolecules 52(10):3805-3812. https://10.1021/acs.macromol.9b00419

41. Xiao Y, Liu P, Wang WJ, Li BG (2021) Dynamically Cross-Linked Polyolefin Elastomers with Highly Improved Mechanical and Thermal Performance. Macromolecules 54(22):10381-10387. https://10.1021/acs.macromol.1c01249

42. Yu B, Yu Y, He G, Shi Y, Wu Y, Liu X (2026) Recyclable fluorinated poly(urethane-urea) vitrimers for high-strength and wear-resistant aramid composites. Compos B Eng 311:113269. https://10.1016/j.compositesb.2025.113269

43. Wang W, Lu X, Li Y, Li X, Sun H, Sun J (2024) Mechanically Robust Reversibly Cross-Linked Polymers with Closed-Loop Recyclability for Use in Flexible Printed Circuit Boards. Adv Funct Mater 34(34):2401822. https://10.1002/adfm.202401822

44. Zhang Y, Yan H, Yu R, Yuan J, Yang K, Liu R, He Y, Feng W, Tian W (2023) Hyperbranched Dynamic Crosslinking Networks Enable Degradable, Reconfigurable, and Multifunctional Epoxy

Vitrimer. Adv Sci 11(2):2306350. https://10.1002/advs.202306350

45. Ding XM, Chen L, Xu YJ, Shi XH, Luo X, Song X, Wang YZ (2023) Robust Epoxy Vitrimer with Simultaneous Ultrahigh Impact Property, Fire Safety, and Multipath Recyclability via Rigid-Flexible Imine Networks. ACS Sustainable Chem Eng 11(39):14445-14456. https://10.1021/acssuschemeng.3c03189

46. Zhao Y, Zhang Y, Bai X, Wang Y, Li Y, Yang S (2025) Sustainable epoxy vitrimer materials with imine and disulfide bonds prepared from epoxidized soybean oils. Ind Crop Prod 225:120435. https://10.1016/j.indcrop.2024.120435

47. Xiang S, Zhou L, Chen R, Zhang K, Chen M (2022) Interlocked Covalent Adaptable Networks and Composites Relying on Parallel Connection of Aromatic Disulfide and Aromatic Imine Cross-Links in Epoxy. Macromolecules 55(23):10276-10284. https://10.1021/acs.macromol.2c01912

48. Dong Z, Lu Y, Li Y, Meng F, Pei L, Zhong S, Yang Y, Wang S, Wang G (2025) Dynamic imine bonds enable closed-loop recycling of high performance PEEK/CF composites. Polym Degrad Stab 242:111693. https://10.1016/j.polymdegradstab.2025.111693

49. Wu G, Zhao Z, Qi S, Tian G, Wu D (2025) Synthesis and characterization of heat-sealable polyimide films with low CTE based on dynamic boronic acid-boroxine. Eur Polym J 236:114172. https://10.1016/j.eurpolymj.2025.114172

50. Wu D, Zhao X, Li X, Dong J, Zhang Q (2023) Dual-crosslinked polyimide dielectric films containing Cu elements for high-temperature film capacitors. Compos Commun 42:101653. https://10.1016/j.coco.2023.101653

51. Alamri A, Wu C, Nasreen S, Tran H, Yassin O, Gentile R, Kamal D, Ramprasad R, Cao Y, Sotzing G (2022) High dielectric constant and high breakdown strength polyimide via tin complexation of the polyamide acid precursor. RSC Adv 12(15):9095-9100. https://10.1039/d1ra06302b

52. Wang J, Yang H, Zhao R, Hou L (2024) In-situ charge polarization effect of copper(II) ion-coordination covalent organic framework induced aerobic PET-ATRP in aqueous phase. J Catal 436:115616. https://10.1016/j.jcat.2024.115616

53. Susheel, Alsubaie AS, Ahmed M, Malhotra SS, Asha, Gupta MK, Ansari A (2025) DFT and TDDFT studies on π-conjugated ligands for copper sensing: analyzing electronic structures and optical performance. J Mol Model 31(11):306-327. https://10.1007/s00894-025-06543-0

54. Wang Z, Wang X, Ren H, Zhu X, Fang Z, Liu Q, Wang K (2025) Stabilizing free radical crosslinked dielectric polymers with metal-organic frameworks: An efficient approach to mitigating dielectric deterioration. Compos Sci Technol 264:111109. https://10.1016/j.compscitech.2025.111109

55. Bei R, Chen K, He Y, Li C, Chi Z, Liu S, Xu J, Zhang Y (2023) A systematic study of the relationship between the high-frequency dielectric dissipation factor and water adsorption of polyimide films. J Mater Chem C 11(30):10274-10281. https://10.1039/d3tc01337e

56. Guo X, Zhang X, Ma L, Li Y, Le J, Fu Z, Lu L, Zhang D (2024) Understanding the adsorption of imidazole corrosion inhibitor at the copper/water interface by ab initio molecular dynamics. Corros Sci 236:112237. https://10.1016/j.corsci.2024.112237

57. Reddy MO, Buddhudu S (2011) Structural, Thermal, Electrical and Magnetic Properties of PVA: Mn^{2+} and PVA: Ni^{2+} Polymer Films. In AIP Conference Proceedings 1372(1):323-331. https://doi.org/10.1063/1.3644464

58. Yang R, Wei R, Li K, Tong L, Jia K, Liu X (2016) Crosslinked polyarylene ether nitrile film as flexible dielectric materials with ultrahigh thermal stability. Sci Rep 6(1):36434. https://10.1038/srep36434

59. Diaham S, Locatelli ML, Lebey T, Dinculescu S (2009) Dielectric measurements in large frequency and temperature ranges of an aromatic polymer. Eur Phys J Appl Phys 49(1):10401. https://10.1051/epjap/2009193

Supplementary Files

This is a list of supplementary files associated with this preprint. Click to download.

- SIPICuSpringer.docx